Available online at www.sciencedirect.com
ScienceDirect
Polymer 48 (2007) 1428–1434
polymer
www.elsevier.com/locate/polymer

(Polystyrene-*g*-polyisoprene)-*b*-polystyrene comb-coil block copolymer in selective solvent

Feng Xu [a], Tingcheng Li [b], Jianfeng Xia [a], Feng Qiu [a,*], Yuliang Yang [a]

[a] *The Key Laboratory of Molecular Engineering of Polymers, Ministry of Education, Department of Macromolecular Science, Fudan University, 200433 Shanghai, China*
[b] *Laboratory of Advanced Materials, Fudan University, 200433 Shanghai, China*

Received 12 September 2006; received in revised form 5 January 2007; accepted 6 January 2007
Available online 11 January 2007

Abstract

Comb-coil block copolymers consisting of two components polystyrene (PS) and polyisoprene (PI) were synthesized through combining TEMPO living free radical polymerization (LFRP) and anionic polymerization using ''grafting-onto'' strategy. Two typical samples with the same backbone but grafted with different numbers and lengths of branches, forming lamellar and cylinder phases, respectively, were investigated. As the selective solvent was added into these block polymers, the micro-structures transformed from disordered or weakly ordered structure into well-organized lamellar structure in the intermediate polymer concentration. The power law behavior of the lamellae space with respect to polymer concentration indicates that the two samples form the well-organized structure through different paths. The sample with longer branch length thus less branch points forms lamellae phase with smaller lamellae space. This difference at lamellae spacing is attributed to the two different ways that the chain assembles.

Keywords: Block copolymer; Microphase separation; Selective solvent

1. Introduction

Nonlinear block copolymers, such as star and graft copolymers, have been attracting growing interests during the past decade. These interests arise from the fact that molecular architecture plays an important role in determining phase behavior of the polymer. For example, in A_2B type the simplest star block copolymers, more than two arms are linked together at one junction point, creating asymmetry in molecular architecture. Compared to AB type linear block copolymer, their morphological transitions occur at higher volume fractions of the component with less arm number [1,2]. For graft block copolymers, it has been recognized that the morphology is dictated by the behavior of the smaller star-like subunits from which they are comprised [3,4].

As illustrated in Fig. 1, comb-coil block copolymer is consisted of a grafted block copolymer BC and a homo-polymer A block. Microphase separation in two length scales has been found in comb-coil block copolymer consisting of three

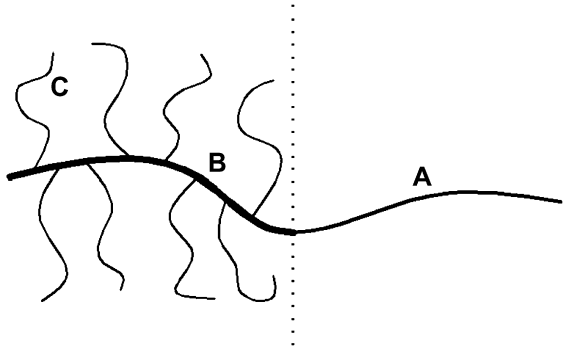

Fig. 1. Sketch of comb-coil block copolymer. (A) homo-polymer block; (B) backbone of the graft block; (C) branches of the graft block.

* Corresponding author. Tel.: +86 021 55664036; fax: +86 021 65640293.
E-mail address: fengqiu@fudan.edu.cn (F. Qiu).

0032-3861/$ - see front matter © 2007 Elsevier Ltd. All rights reserved.
doi:10.1016/j.polymer.2007.01.008

components in experiments [5–7]. Here, we are interested in comb-coil block copolymer consisted of two components, in which A and B are of the same species. Weak segregation theory predicted that microphase separation at two length scales, i.e., between the comb part and the homo-polymer block, or between the branches and the backbone, may also occur in comb-coil block copolymers with only two components [8,9].

However, it is difficult to directly monitor how the polymer chains assemble in each domain of microphase separation in the experiment. In order to overcome this difficulty, we introduce selective solvent into the comb-coil block copolymer. Adding a solvent will change the domain size and even cause microphase transition [10,11], depending on the selectivity of the solvent. The change of domain size can be described by a power law in terms of the volume fraction of the polymer $\phi_P : d \sim \phi_P^{-\beta}$, where in general $\beta < 0$ for nonselective solvents. Nonselective solvents reduce d by screening the unfavorable interactions between the dissimilar segments at the microdomain interface. For selective solvents, especially strongly selective solvents, which are precipitants for one of the blocks, β may become positive [12]. Through the swelling process, information on polymer chain assembly may be obtained. The morphologies of the solutions were characterized by small angle X-ray scattering (SAXS). The purpose of this article is to present the morphologies of block copolymers with complex architecture in selective solvent, thus to get further understanding on chain assembly of such polymers.

2. Experimental section

2.1. Synthesis

The synthesis of the comb-coil block copolymer was carried out in three steps, following Refs. [4,13], as shown in Scheme 1. First, styrene (St) and chloromethylstyrene (CMS) were copolymerized by living free radical polymerization (LFRP) to incorporate chloromethyl groups into the backbone. The chlorine atoms are randomly distributed along the PS chain due to similar reactivity of St and CMS (the reactivity ratio for St:CMS is 0.72:1.08). Then, poly(St-*co*-CMS)-*b*-St was synthesized by LFRP of styrene and the random copolymer. Finally, comb-coil block copolymer was obtained using graft-onto method by coupling the living anions of polyisoprene created by anionic polymerization with the PS backbone. Fractionation with toluene as solvent and methane as non-solvent is effective to isolate the comb-coil block copolymer product.

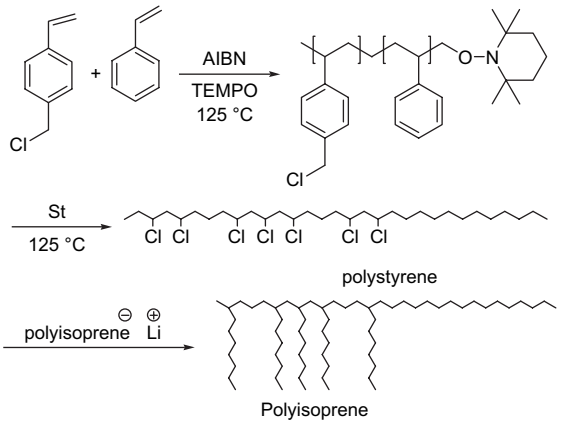

Scheme 1. Polymerization procedure of the comb-coil block copolymer.

The graft-onto strategy used in our synthesis allows characterization of the backbone and the branch separately. Molecular weight and polydispersity of the linear polymers, i.e., PS backbone and PI branch, were characterized by gel permeation chromatography (GPC). The molecular weight and molecular weight distribution of the comb-coil block polymers were characterized by a GPC coupled (static) laser light scattering technique. The number of PI branches was estimated from the number-average molecular weight of each part. The sample characteristics are compiled in Table 1.

To describe the molecular architecture, the following notation is used: S_m-*g*-$I_{n\times p}$-*b*-S_l, where S and I stand for PS and PI, respectively, m, n and l give the number-average molecular weight of each part; p is the number of PI branch points.

2.2. Sample preparation

Thin films of the comb-coil copolymers were cast from 10 wt% solutions in toluene (a good solvent for both PS and PI). The evaporation of the solvent was carried out slowly in air at room temperature for one week and then in a vacuum oven at room temperature for two days.

The solvent dimethyl phthalate (DMP) was purified according to the process in literature [11]. Solutions were prepared gravimetrically, using methylene chloride as a co-solvent. The co-solvent was evaporated at room temperature for three

Table 1
Characterization data of comb-coil block copolymers: molecular weight of PS backbone and PI branches, number of branch points, total molecular weight, polydispersity (PDI), and volume fraction of PS

Samples	PS backbone		PI branch		Comb-coil block copolymer				
	$10^{-3}\overline{M}_{n,cb}$	$\overline{M}_w/\overline{M}_n$	$10^{-3}\overline{M}_{n,PI}$	$\overline{M}_w/\overline{M}_n$	$10^{-3}\overline{M}_{w,cc}$ [a]	$10^{-3}\overline{M}_{n,cc}$ [a]	$\overline{M}_w/\overline{M}_n$	X [b]	ϕ_{PS} [c]
(S_{20}-*g*-$I_{2.6\times13}$)-*b*-S_{27}	47	1.20	2.6	1.03	95	81	1.17	13	0.54
(S_{20}-*g*-$I_{4.3\times9}$)-*b*-S_{27}	47	1.20	4.3	1.05	94	86	1.10	9	0.50

[a] Obtained by GPC/LS system at 35 °C in THF.
[b] Number of branches determined by the ratio: $X = (\overline{M}_{n,cc} - \overline{M}_{n,cb})/\overline{M}_{n,PI}$.
[c] Corrected by the densities of PS and PI.

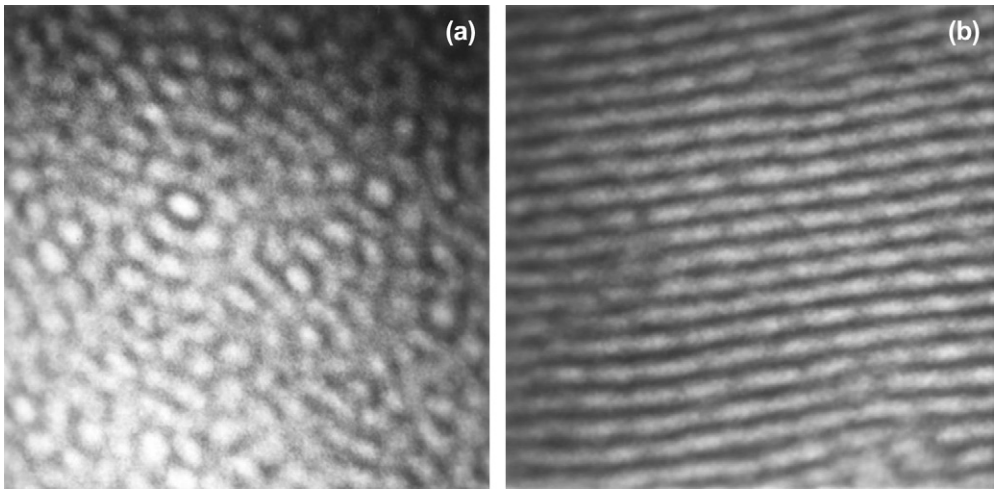

Fig. 2. TEM images of (a) (S_{20}-g-$I_{2.6\times13}$)-b-S_{27} and (b) (S_{20}-g-$I_{4.3\times9}$)-b-S_{27}. The area of each image is 0.5 μm × 0.5 μm.

days, followed by evaporation in vacuum for one day until constant weight was achieved. The measurements were carried out under room temperature, so no antioxidant was used. Concentrations were converted to polymer volume fraction, ϕ_P, assuming volume additivity and densities of 1.05, 0.904, and 1.16 g/mL for PS, PI, and DMP, respectively.

2.3. Techniques

The morphology of (PS-g-PI)-b-PS melt was observed by Hitachi H-800 transmission electron microscope (TEM). The films were microtomed at −95 °C. The ultra-thin sections were picked onto the copper grids coated with carbon-supporting films followed by staining by exposure to the vapor of 2% osmium tetra-oxide (OsO_4) solution for 2 h. OsO_4 is a preferential staining agent for PI blocks, so the PI phase appears dark in the TEM micrographs.

The small angle X-ray scattering (SAXS) measurements were carried out with a Bruker Nanostar U System, with an incident X-ray wavelength of 1.54 Å. The collimation system consists of two cross coupled Gobel Mirrors and four pinholes. A Histar area detector (Siemens) filled with pressurized xenon and CO_2 gases was used to record the SAXS scattering patterns, at a sample to detector distance of 106.1 cm. Two-dimensional images were corrected for detector response, azimuthally averaged, and placed on an intensity vs. scattering vector ($q = 4\pi \sin(\theta/2)/\lambda$) scale. We focus on the physical quantities obtainable from SAXS: the scattering peak intensity I, the scattering vector q^*, which gives the maximum scattered intensity or characteristic length,

$$d \equiv \frac{2\pi}{q^*}$$

All data obtained from the SAXS experiments have been repeated for at least three times.

3. Results and discussion

The TEM images and SAXS profiles of (S_{20}-g-$I_{2.6\times13}$)-b-S_{27} and (S_{20}-g-$I_{4.3\times9}$)-b-S_{27}, which are composed by the same PS backbone but different number of branch points and the length of branches, are shown in Figs. 2 and 3, respectively. The ratios of q_n/q^* for the series of peaks in a diffraction pattern are characteristic of the lattice symmetry when Bragg scattering is present, where the scattering vector of the Bragg peak with the lowest scattering angle is referred to as q^*, and q_n are the series of peaks, in the order of increasing scattering angle, beginning with q^*. The TEM image of the sample of (S_{20}-g-$I_{2.6\times13}$)-b-S_{27} shows PS packed hexagonal cylinder with defects. The SAXS data display a second broad maximum centered at q_n/q^* equal to $\sqrt{3}$, which is consistent with the symmetry of a hexagonal morphology. However, (S_{20}-g-$I_{4.3\times9}$)-b-S_{27} assembles into lamellae with the q_n/q^* ratio close

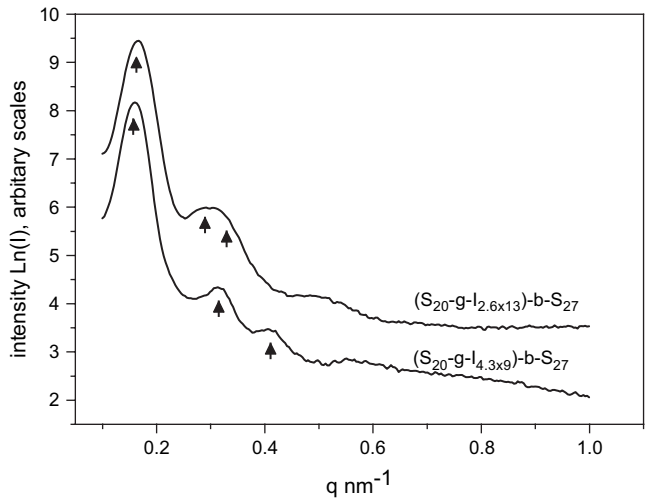

Fig. 3. Small angle X-ray scattering profiles of (S_{20}-g-$I_{2.6\times13}$)-b-S_{27} and (S_{20}-g-$I_{4.3\times9}$)-b-S_{27}. Possible reflections are labeled with upwards arrows.

to 1:2:2.6. The discrepancy of the third reflection with typical scattering profiles for lamellae may be due to the coexistence of cylinder structure in some areas.

Why do the two samples with similar PS volume fraction form different micro-structures? According to the weak segregation theory by Nap and ten Brinke, the way of microphase separation is determined by the homo-polymer block length and the space between branches or branch length. Therefore, different chain architectures may be the answer to the question. However, no enough information of how different blocks assemble in the melt can be obtained in TEM and SAXS experiments. To further understand the underlying mechanism, swelling experiments using dimethyl phthalate (DMP), a strong PS-selective solvent with extremely low vapor pressure (less than 0.01 mmHg at room temperature), were carried out. Fig. 4 shows SAXS profiles of the (S_{20}-*g*-$I_{4.3\times9}$)-*b*-S_{27} DMP solutions. The phase behavior can be divided into three regions. In the first region, shown in Fig. 4(a), when $\phi_P > 0.6$, the scattering profiles of the solutions display a second broad maximum centered at $q_2/q^* \approx 2$, which indicates that the copolymer assembles into lamellae phase, but the structures are not well organized. In the second region, as in Fig. 4(b), when $0.4 < \phi_P < 0.6$, all the SAXS profiles show typical lamellar phase with reflection ratios of q_n/q^* equal to 1:2:3:4… Relatively sharp subreflections indicate well-organized phase structures and sharp boundary. In the third region, when $\phi_P < 0.4$, the SAXS profiles indicate a disordered phase (shown in Fig. 4(c)). According to the studies on diblock copolymer in DMP [13], we believe that the copolymers assemble into micelles in this region and the reflections of the micelles have exceeded the limit of the present measurement.

Similar scattering profiles for (S_{20}-*g*-$I_{2.6\times13}$)-*b*-S_{27} DMP solutions were obtained, as shown in Fig. 5. In the second region, when $0.64 > \phi_P > 0.45$, the copolymer solutions display a well-organized lamellar phase. With the increase of solvent, when $\phi_P < 0.45$, the ordered phases disappear. However, the phase behavior is more complex in region (a) of the (S_{20}-*g*-$I_{2.6\times13}$)-*b*-S_{27} DMP solution than that of (S_{20}-*g*-$I_{4.3\times9}$)-*b*-S_{27}. As selective solvent is added into the polymer, the morphology of (S_{20}-*g*-$I_{2.6\times13}$)-*b*-S_{27} turns to lamellae from cylinder. Due to the low mobility of polymer chains in the highly concentrated solutions, it is difficult to accurately locate the boundary of the transition.

The above analysis is well supported by a power law dependence ($d \sim \phi_P^{-\beta}$), which is fit to the region in which no structural phase transition happens. Fig. 6 shows that the domain size increases with the increase of the solvent concentration. For (S_{20}-*g*-$I_{4.3\times9}$)-*b*-S_{27} DMP solutions, the data from regions (a) and (b) fit to the power law very well. For (S_{20}-*g*-$I_{2.6\times13}$)-*b*-S_{27} DMP solutions, only data from region (b) fit to the power law. From the slope of the lines, we obtain $\beta = 0.40 \pm 0.04$ for (S_{20}-*g*-$I_{2.6\times13}$)-*b*-S_{27} DMP solutions and $\beta = 0.30 \pm 0.02$ for (S_{20}-*g*-$I_{4.3\times9}$)-*b*-S_{27} DMP solutions.

According to the TEM images and SAXS profiles in Figs. 2 and 3, cylinder phase was obtained in (S_{20}-*g*-$I_{2.6\times13}$)-*b*-S_{27}. The volume fraction of the PS homo-polymer in (S_{20}-*g*-$I_{2.6\times13}$)-*b*-S_{27} is 0.31, which is located in cylinder phase region in the phase diagram of an AB diblock copolymer [14]. In contrast, the volume fraction of the PS homo-polymer block in (S_{20}-*g*-$I_{4.3\times9}$)-*b*-S_{27} is 0.29, which is slightly lower

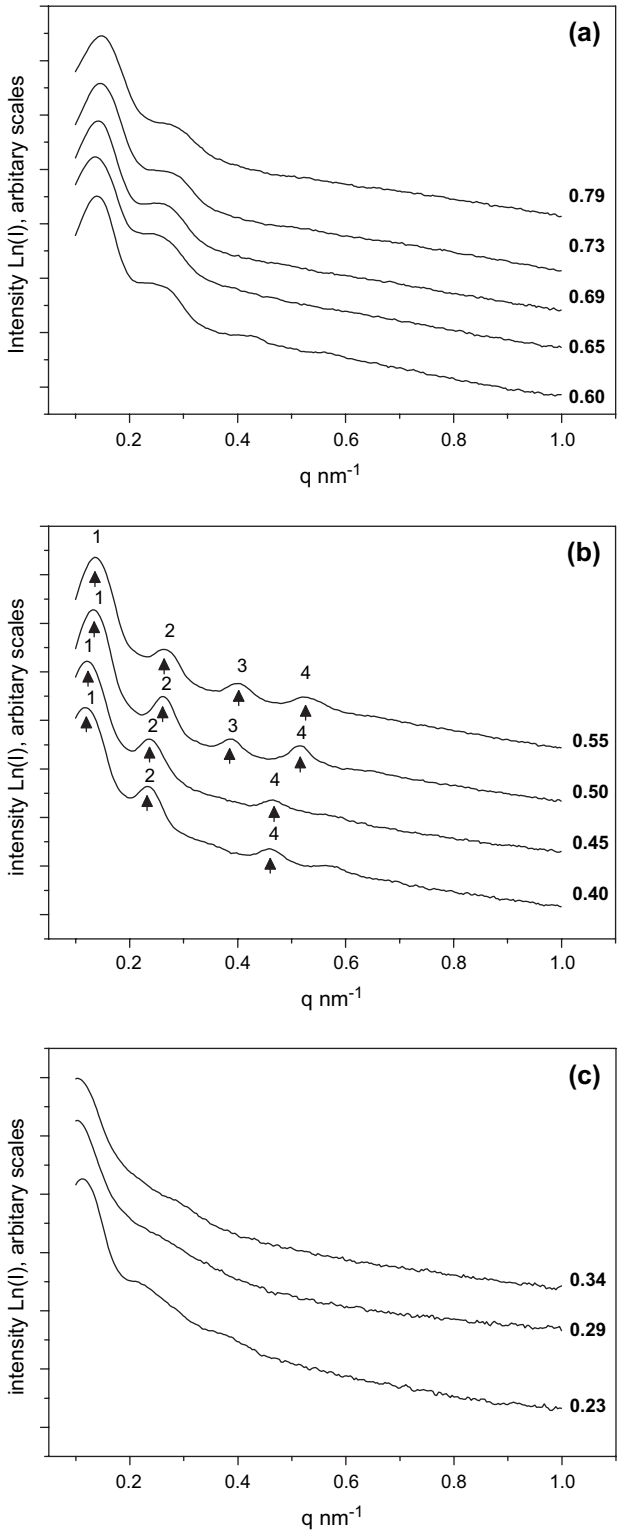

Fig. 4. SAXS profiles of (S_{20}-*g*-$I_{4.3\times9}$)-*b*-S_{27} DMP solutions. Each curve is labeled with the concentration (volume fraction of the polymer in solutions).

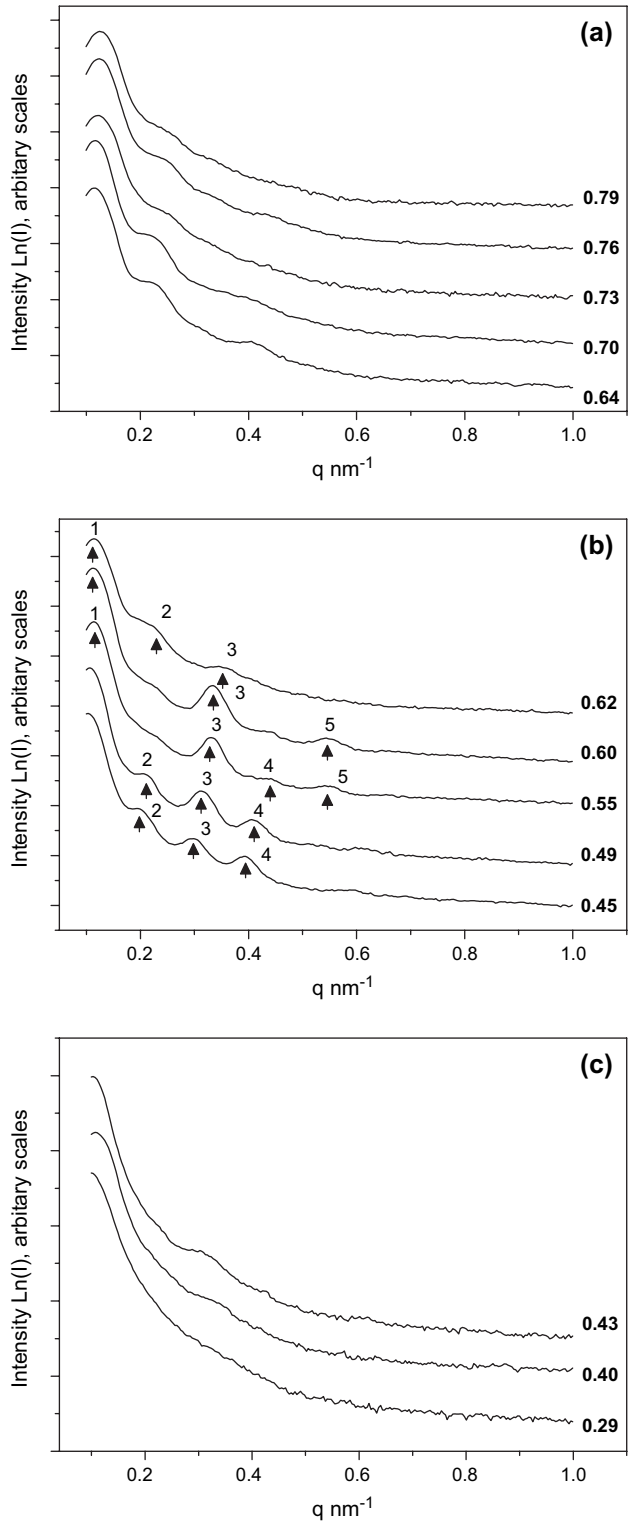

Fig. 5. SAXS profiles of $(S_{20}\text{-}g\text{-}I_{2.6\times13})\text{-}b\text{-}S_{27}$ DMP solutions. Each curve is labeled with the concentration (volume fraction of the polymer in solutions).

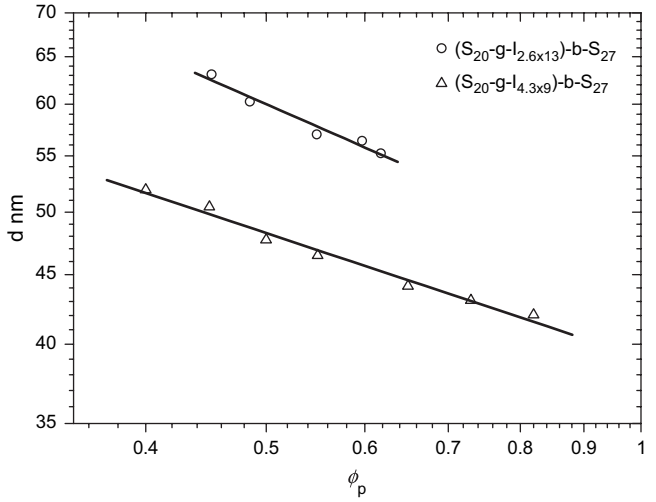

Fig. 6. Double-logarithmic plot of the concentration dependence of domain size at room temperature.

than that in $(S_{20}\text{-}g\text{-}I_{2.6\times13})\text{-}b\text{-}S_{27}$. Therefore, one would also expect cylinder rather than lamellae will be preferential for $(S_{20}\text{-}g\text{-}I_{4.3\times9})\text{-}b\text{-}S_{27}$ if microphase separation occurs between the comb block and the homo-polymer S_{27} block. However, a lamellae phase is obtained, which suggests that $(S_{20}\text{-}g\text{-}I_{4.3\times9})\text{-}b\text{-}S_{27}$ may have microphase separation between the S backbone (both S_{20} and S_{27}) and the I branches. Indeed, the total volume fraction of the S backbone in the lamellae is 0.5. The illustrations of the chain assembly in the melts of the two samples are shown in Fig. 7.

As the PS-selective solvent is added into the samples, the domains consisted mainly of PS are swelled, leading to the increase of the domain size and even microphase transition, as shown in Fig. 8. In fact, the positive value of β indicates the increase of the lamellar space with the addition of the selective solvent. Interestingly, for $(S_{20}\text{-}g\text{-}I_{2.6\times13})\text{-}b\text{-}S_{27}$, the solvent expands the homo-polymer PS (volume fraction 0.31) packed cylinders and transform the structure into lamellae. We believe the reason is that if the PS-selectivity of DMP is sufficiently strong (the estimated Flory–Huggins interaction parameters between DMP and PS $\chi_{PS,DMP} = 0.72$, and between DMP and PI $\chi_{PI,DMP} = 1.9$ at room temperature [15]), the addition of the solvent is equivalent to the increasing the volume fraction of PS [11,16]. It is well known that in an asymmetric diblock copolymer melt, the increase of the volume fraction of the minor component is able to cause a sphere-to-cylinder-to-lamella transition. Indeed, a calculation for linear diblock copolymer solution based on self-consistent field theory indicates that when a strongly selective solvent is added, similar sequence of transition appears [17]. We believe here that for nonlinear diblock copolymers this basic concept also applies.

Comparing the well-organized lamellae in the intermediate concentration of the two samples, we can find that the lamellae width of $(S_{20}\text{-}g\text{-}I_{2.6\times13})\text{-}b\text{-}S_{27}$ ($d = 60$ nm) is 25% larger than that of $(S_{20}\text{-}g\text{-}I_{4.3\times9})\text{-}b\text{-}S_{27}$ ($d = 48$ nm), which is assumed to be the consequence of microphase separation through two different paths. Since the PS backbone and PS homo-polymer are much longer than each PI branch, it is understandable that microphase separation between comb block and homo-polymer block, as for $(S_{20}\text{-}g\text{-}I_{2.6\times13})\text{-}b\text{-}S_{27}$, would result in larger domain size.

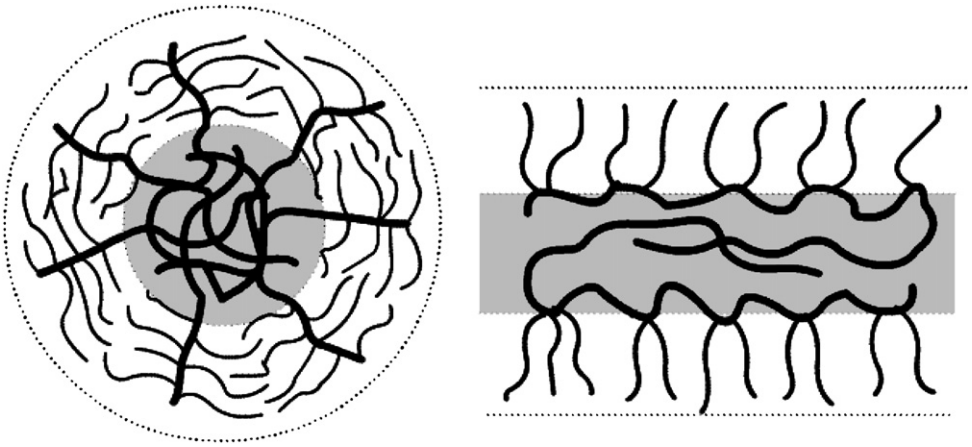

Fig. 7. Illustrations of possible chain assembly in melt for (S_{20}-*g*-$I_{2.6\times13}$)-*b*-S_{27} (left) and (S_{20}-*g*-$I_{4.3\times9}$)-*b*-S_{27} (right).

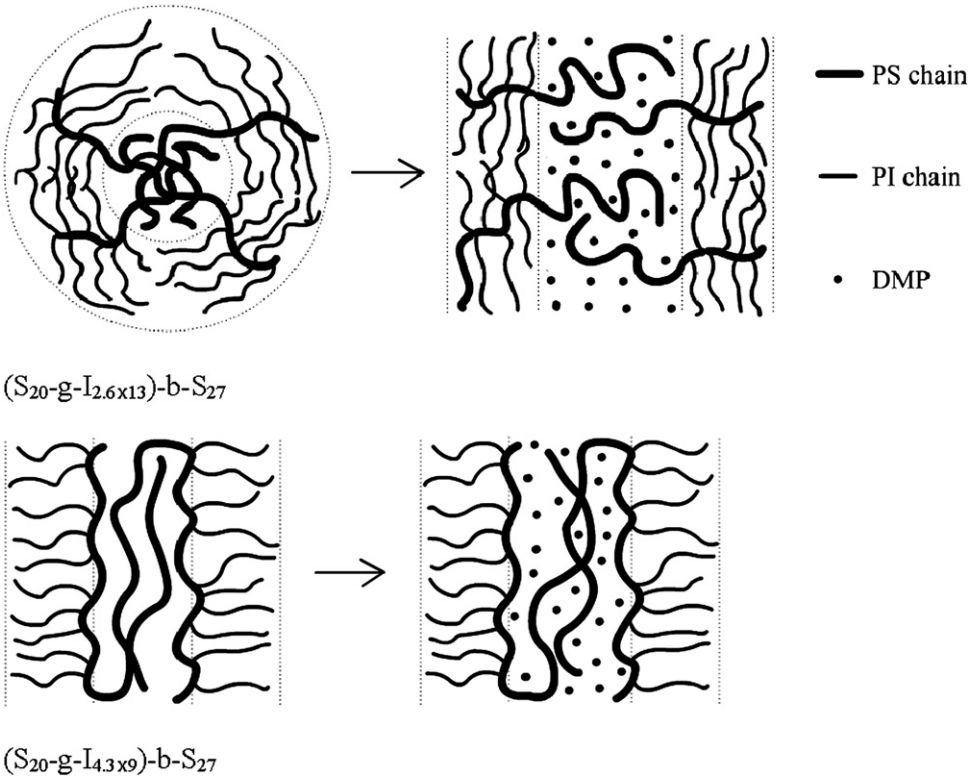

Fig. 8. Illustration of the swelling processes.

4. Conclusions

We investigated the phase structures of two comb-coil diblock copolymers consisting of PS backbones and PI branches, in the PS-selective solvent DMP. The samples were successfully synthesized through a combination of free radical polymerization and living anionic polymerization using the ''grafting-onto'' strategy. The two samples with similar volume fraction of PS show different morphologies in bulk, due to two ways of microphase separation. As the selective solvent is added into the copolymers, both of the two samples form well-organized lamellae phase in the intermediate concentrations. A power law dependence of the domain size vs. volume fraction of the diblock copolymer in solution is found: $d \sim \phi_P^{-\beta}$, $\beta = 0.4$ and 0.3 for (S_{20}-*g*-$I_{2.6\times13}$)-*b*-S_{27} and (S_{20}-*g*-$I_{4.3\times9}$)-*b*-S_{27}, respectively. The different lamellae space shows that the polymer chains assemble also in two ways in the solution of the two comb-coil diblock copolymers.

Acknowledgements

We gratefully acknowledge the financial support from the National Basic Research Program of China (G2005CB623800) and the NNSF of China (Grant Nos. 20625413 and 20490220). F.Q. acknowledges Ministry of Education of China (FANEDD 200225).

Appendix A. Supplementary data

Supplementary data associated with this article can be found in the online version, at doi:10.1016/j.polymer.2007.01.008.

References

[1] Chrissopoulou K, Harville S, Anastasiadis SH, Fytas G, Mays JW, Hadjichristidis N. Journal of Polymer Science, Part B: Polymer Physics 1999;37(24):3385.

[2] Lee C, Gido SP, Pitsikalis M, Mays JW, Tan NB, Trevino SF, et al. Macromolecules 1997;30(13):3732.

[3] Beyer FL, Gido SP, Buschl C, Iatrou H, Uhrig D, Mays JW, et al. Macromolecules 2000;33(6):2039.

[4] Xenidou M, Beyer FL, Hadjichristidis N, Gido SP, Tan NB. Macromolecules 1998;31(22):7659.

[5] Ruokolainen J, Makinen R, Torkkeli M, Makela T, Serimaa R, ten Brinke G, et al. Science 1998;280(5363):557.

[6] Nandan B, Lee CH, Chen HL, Chen WC. Macromolecules 2005;38(24):10117.

[7] Ruokolainen J, Saariaho M, Ikkala O, ten Brinke G, Thomas EL, Torkkeli M, et al. Macromolecules 1999;32(4):1152.

[8] Nap RJ, Kok C, ten Brinke G, Kuchanov SI. The European Physical Journal E 2001;4(4):515.

[9] Nap RJ, ten Brinke T. Macromolecules 2002;35(3):952.

[10] Lodge TP, Hanley KJ, Pudil B, Alahapperuma V. Macromolecules 2003;36(3):816.

[11] Lodge TP, Pudil B, Hanley KJ. Macromolecules 2002;35(12):4707.

[12] Lai CJ, Russel WB, Register RA. Macromolecules 2002;35(10):4044.

[13] Hanley KJ, Lodge TP, Huang CI. Macromolecules 2000;33(16):5918.

[14] Leibler L. Macromolecules 1980;13:1602.

[15] The Flory–Huggins parameters can be estimated from the solubility parameters of the components of a polymer solution: $\chi_{AB} = (V_m/RT)(\delta_A - \delta_B)^2$, where δ_A and δ_B are the Hildebrand solubility parameters of the polymer and solvent. V_m is the molar volume of the solvent, which can be obtained from its density and molecular weight. For DMP, $V_m = 167\ cm^3/mol$. The solubility parameters of the polymers and solvent are $\delta_{PS} = 9.1(cal/cm^3)^{1/2}$, $\delta_{PI} = 8.1(cal/cm^3)^{1/2}$, and $\delta_{DMP} = 10.4-10.7(cal/cm^3)^{1/2}$ (data from Brandrup J, Immergut EH, Grulke EA. Polymer handbook. 4th ed. New York: Wiley; 1999. p. 3). Then at room temperature $\chi_{PS,DMP} = 0.72$ and $\chi_{PI,DMP} = 1.9$, indicating DMP is a PS-selective solvent.

[16] Sadron C, Gallot B. Die Makromolekulare Chemie 1973;164:301.

[17] Huang CI, Lodge TP. Macromolecules 1998;31:3556.